

AI-driven Characterization of Solid Pulmonary Nodules on CT Imaging for Enhanced Malignancy Prediction in Small-sized Lung Adenocarcinoma

Yujin Kudo,¹ Taiyo Nakamura,¹ Jun Matsubayashi,² Akimichi Ichinose,³
Yushi Goto,¹ Ryosuke Amemiya,¹ Jinho Park,⁴ Yoshihisa Shimada,¹
Masatoshi Kakihana,¹ Toshitaka Nagao,² Tatsuo Ohira,¹ Jun Masumoto,³
Norihiko Ikeda¹

Abstract

This study utilized artificial intelligence (AI) to distinguish solid nodules from ground-glass nodules in 246 patients with lung adenocarcinoma ≤ 2 cm in size. The classification of solid/non-solid nodules by AI was well correlated with pathological findings, demonstrating malignant potential in AI-identified solid nodules. This approach enhances the accuracy of preoperative diagnosis and improves treatment strategies.

Objectives: Distinguishing solid nodules from nodules with ground-glass lesions in lung cancer is a critical diagnostic challenge, especially for tumors ≤ 2 cm. Human assessment of these nodules is associated with high inter-observer variability, which is why an objective and reliable diagnostic tool is necessary. This study focuses on artificial intelligence (AI) to automatically analyze such tumors and to develop prospective AI systems that can independently differentiate highly malignant nodules. **Materials and methods:** Our retrospective study analyzed 246 patients who were diagnosed with negative clinical lymph node metastases (cN0) using positron emission tomography-computed tomography (PET/CT) imaging and underwent surgical resection for lung adenocarcinoma. AI detected tumor sizes ≤ 2 cm in these patients. By utilizing AI to classify these nodules as solid (AI_solid) or non-solid (non-AI_solid) based on confidence scores, we aim to correlate AI determinations with pathological findings, thereby advancing the precision of preoperative assessments. **Results:** Solid nodules identified by AI with a confidence score ≥ 0.87 showed significantly higher solid component volumes and proportions in patients with AI_solid than in those with non-AI_solid, with no differences in overall diameter or total volume of the tumors. Among patients with AI_solid, 16% demonstrated lymph node metastasis, and a significant 94% harbored invasive adenocarcinoma. Additionally, 44% were upstaging postoperatively. These AI_solid nodules represented high-grade malignancies. **Conclusion:** In small-sized lung cancer diagnosed as cN0, AI automatically identifies tumors as solid nodules ≤ 2 cm and evaluates their malignancy preoperatively. The AI classification can inform lymph node assessment necessity in sublobar resections, reflecting metastatic potential.

Clinical Lung Cancer, Vol. 25, No. 5, 431–439 © 2024 Elsevier Inc. All rights reserved.

Keywords: Artificial intelligence, Ground-glass nodule, Three-dimensional imaging, Lung adenocarcinoma, Sublobar resection

Abbreviations: AI, artificial intelligence; GGN, ground-glass nodule; NSCLC, non-small cell lung cancer; FDG, F-fluorodeoxyglucose; EBUS-TBNA, endobronchial ultrasound-guided transbronchial needle aspiration; PET/CT, positron emission tomography-computed tomography; HRCT, high-resolution computed tomography; CAD, computer-aided detection; AUC, area under the curve; VPI, visceral pleural invasion; BVI, blood vessel invasion; EVG, Elastica van Gieson; CEA, carcinoembryonic antigen; IQR, Interquartile range; CTR, consolidation tumor ratio; NS, not significant.

¹Department of Surgery, Tokyo Medical University, Japan

²Department of Anatomic Pathology, Tokyo Medical University, Japan

³Fujifilm Corporation, Japan

⁴Department of Radiology, Tokyo Medical University, Japan

Submitted: Mar 16, 2024; Revised: Apr 21, 2024; Accepted: Apr 24, 2024; Epub: 27 April 2024

Address for correspondence: Yujin Kudo, M.D. Ph.D., Department of Surgery, Tokyo Medical University, 6-7-1 Nishishinjuku, Shinjuku-ku, Tokyo 160-0023, Japan.

E-mail contact: ykudo@tokyo-med.ac.jp

Introduction

Lung cancer remains one of the most challenging malignancies to treat and is the leading cause of cancer-related deaths worldwide.¹ From a pathologic perspective, despite poor prognosis, developments in lung cancer research have led to the detailed classification of lung cancers.^{2,3} It has facilitated the development of minimally invasive surgical techniques such as segmentectomy⁴⁻⁶ and improvements in perioperative therapy.^{7,8} These advances have significantly improved the management and outcome of patients with lung cancer, highlighting the importance of early, and accurate diagnosis to optimize treatment strategies.

Evidence is accumulating to support the efficacy of sublobar resection in small-sized lung cancers, particularly tumors ≤ 2 cm in diameter.^{4,5} This surgical approach is gaining attention due to its potential advantages in preserving lung function and improving postoperative quality of life. However, the selection criteria for sublobar resection often require the absence of lymph node metastases, which can be determined preoperatively or intraoperatively. This poses a significant challenge because there are limitations to lymph nodes that can be resected in segmentectomy and may affect the comprehensive assessment of lymph node metastases.

Preoperative radiological imaging plays a crucial role in evaluating small-sized lung cancer. Additionally, ground-glass nodules (GGNs) are associated with a favorable prognosis, while solid nodules are reported to have poor prognoses with higher malignancies and more frequent lymph node metastases.⁹⁻¹⁵ However, distinguishing between GGN and substantial nodules and assessing the presence of GGN often relies on subjective interpretation and can vary significantly from individual physician to physician. This variability emphasizes the necessity for more objective and reliable diagnostic tools to improve preoperative assessment and lead to surgical strategies.

AI analysis offers a promising solution to these challenges. We have integrated AI into the preoperative radiological imaging process for lung cancer, allowing automated 3D analysis of nodules and GGNs and reporting their relationship to prognosis.¹⁶⁻¹⁸ We aimed to objectively assess the correlation between tumor pathology and clinical outcomes by automatically measuring tumor sizes and categorizing nodules as solids or those containing a GGN component. The purpose of this study is to investigate the potential of AI to improve the accuracy of preoperative radiologically diagnostic imaging in predicting pathological malignancy and lymph node metastasis in small-sized non-small cell lung cancer (NSCLC), thereby contributing to more informed decision-making in the treatment of this challenging disease.

Material and Methods

Study Population

This study retrospectively examined 246 patients who underwent pulmonary resection for small-sized lung adenocarcinoma, defined as ≤ 2 cm, at Tokyo Medical University Hospital from 2017 to 2021. Tumor diameters were assessed using AI Software Beta Version in Synapse Vincent system (Fujifilm, Tokyo, Japan), an advanced imaging analysis system that utilizes AI for accurate measurement. This system provided an objective and standardized approach to determining tumor size eligibility for the study. Patients

who received preoperative chemotherapy or radiotherapy, or both, as well as those with low-grade malignancies, were excluded. The preoperative stage was determined by high-resolution computed tomography (HRCT), ¹⁸F-fluorodeoxyglucose (FDG) PET/CT, or endobronchial ultrasound-guided transbronchial needle aspiration (EBUS-TBNA) followed by histological analysis. For clinical node assessment, no lymph node metastasis was defined as enlarged lymph nodes of < 10 mm in the short axis on CT images or negative FDG uptake by the lymph nodes on PET/CT images. Invasive examinations for mediastinal lymph node staging, such as EBUS-TBNA, were preoperatively conducted when the clinical node criteria indicated radiologically positive metastasis, allowing for the implementation of EBUS-TBNA. Clinical staging was performed based on TNM classification (8th edition).^{19,20} The Institutional Review Board of our hospital approved the protocol for data collection and analyses, and the need to obtain written informed consent from each patient was waived (study approval no.: SH3951).

Artificial Intelligence Analysis with Synapse Vincent

In our previous work, we have reported AI analysis of pulmonary nodules using Synapse Vincent.^{16,17} This segmentation algorithm is based on a 3D convolutional neural network using a modified U-net architecture. This network consisted of 17 convolutional layers. The latest version of the development software has enhanced capabilities, automating the detection and extraction of pulmonary nodules across the entire lung field. With the activation of the computer-aided detection (CAD) system, it can identify and calculate the volumes of GGNs and solid lesions, along with their respective proportions. The system automatically calculates 17 3D radiological parameters, including the maximum diameter of the tumor, the solid component, and the CT values.

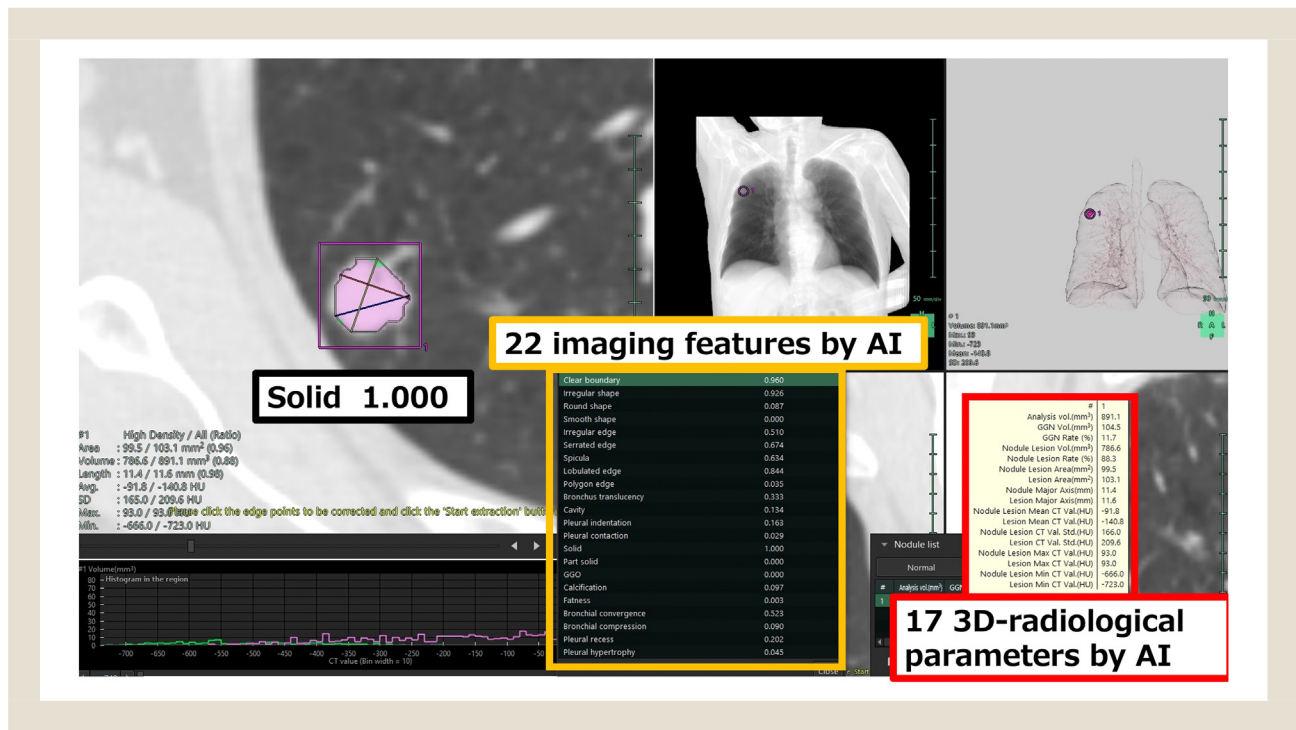
Additionally, this AI software beta version in the Synapse Vincent system facilitates the characterization of pulmonary nodules by assessing 22 imaging features, quantifying each with a confidence score ranging from 0 to 1. A screenshot of this analytic process is provided (Figure 1). The 22 imaging features were based on the labeling of 5118 tumors. The datasets of the development process were divided into training, validation, and test sets. The trained model yielded a mean area under the curve (AUC) score of 0.93 for all features in the test dataset.^{21,22} This AI lung nodule analysis model uses a convolutional neural network based on VGG-16 and consists of 12 convolution layers, with 4 layers removed from the output side of the VGG-16. To extract 3D imaging features, 3D convolution was used for all convolution layers.

In this study, three of the 22 factors were focused on: solid nodules, partially solid GGN, and GGN. The confidence scores for these three factors indicated the plausibility of the AI's judgments, resulting in a total score of 1. The AI analyzed these three factors using the same method as the remaining 19 factors. However, the scoring relationship among these 3 factors appeared unique as it assessed the characteristics of the nodules.

Radiological Evaluation

HRCT images of the whole lung were acquired using the previous settings described in.²³ Briefly, HRCT images with a 1.25-mm thickness were obtained of the entire lung. The size of the whole

Figure 1 Screenshot of AI analysis and a representative “AI_solid” pulmonary nodule case. The screenshot shows the evaluation of a pulmonary nodule by AI, detailing the calculation of 22 imaging features and 17 three-dimensional radiological parameters. AI assigned a confidence score of 1.000 to a solid nodule, which was classified as “AI_solid”.



tumor and solid tumor were preoperatively measured from the HRCT images. The solid tumor size was defined as the maximum dimension of the solid component of the lung window, excluding GGNs. The CTR (%) was defined as the maximum dimension of consolidation in the lung window setting divided by the maximum dimension of the tumor in the lung window setting. The diameter of each tumor was meticulously measured by a team of several attending thoracic surgeons, including a board-certified physician, to ensure the accuracy and reliability of the data. These measurements were approved at a multidisciplinary team conference involving radiologists, thoracic surgeons, and oncologists.

Pathological Evaluation

All resected specimens were formalin-fixed and stained with hematoxylin and eosin using routine procedures. Two experienced pathologists, Jun Matsubayashi and Toshitaka Nagao, reviewed the surgical specimens. TNM classification was performed according to the Union for International Cancer Control and the American Joint Committee on Cancer staging system (8th edition).²⁰ Histopathological analyses were performed according to the World Health Organization criteria (5th edition).²⁴ For detailed analyses of visceral pleural invasion (VPI), blood vessel invasion (BVI), and lymphatic permeation.^{23,25} Elastica van Gieson (EVG) and D2-40 staining were routinely used to evaluate histological structures and tumor invasion. VPI was defined as tumor invasion beyond the elastic layer of the pleura. BVI and lymphatic permeation were deter-

mined by identifying conspicuous clusters of intravascular cancer cells surrounded by blood and lymphatic vessels.

Statistical Analysis

Continuous variables between two categories were analyzed using the Mann–Whitney U-test when normality tests indicated a non-normal distribution for the variables. Univariable analysis for survival was performed among the different groups. In the multivariable analysis, the backward stepwise procedure was performed for pre-operative variables such as radiological factors or carcinoembryonic antigen (CEA), using the Cox proportional hazards model to control for bias due to confounding. An adjusted significance level of 0.05 was used to exclude a variable from the model. The likelihood ratio test was performed to analyze interactions based on the variables selected in the final model. All variables, including radiological parameters, CEA, and pathological parameters, were available, although missing data were excluded from the analysis.

Subgroup analysis was performed because histological differences might affect radiological profiles. Bonferroni *P*-value adjustment was used to control for multiple comparisons. A *P*-value of <.025 indicates a statistically significant difference between groups in each analysis. Furthermore, the study was exploratory, and there was no prior planning to adjust for multiple comparisons; the *P*-values are interpreted as descriptive rather than confirmatory. All statistical calculations were performed using SPSS statistical software (version 27.0; SPSS, Inc., Armonk, NY, USA). Graphs were generated using

Table 1 Patient characteristics (n = 246)

Variable	Cases (%)
Sex (Men/women)	108 (43.9) / 138 (56.1)
Median age (IQR)	66 (56-73) years
Smoking habits (Ever/never)	140 (56.9) / 106 (43.0)
Median maximum tumor diameter on imaging (IQR)	1.4 (1.2-1.6) cm
Median maximum solid component diameter on imaging (IQR)	1.0 (0.5-1.3) cm
Median CTR (IQR)	0.68 (0.37-1.00)
Type of surgical procedure (Lobectomy/Sublobar)	174 (70.7) / 72 (29.2)
Median pathological tumor diameter (IQR)	1.5 (1.2-1.8) cm
Median pathological invasion diameter (IQR)	0.8 (0.1-1.5) cm
Lymph node involvement (pN0/pN1/pN2)	229 (93.1) / 10 (4.1) / 7 (2.8)
Pathological factors (ly/v/pl/pm)	46(18.6) / 31(12.6) / 20(8.1) / 6(2.4)
Predominant subtypes (AIS, MIA/invasive adenocarcinoma)	103(41.8) / 143 (58.2)
Pathological stage (0 / IA1-2 / IA3-III)	19(7.7) / 183(74.4) / 44(17.9)

GraphPad Prism (version 9.1.0.; GraphPad Software, San Diego, CA, USA) and SPSS statistical software.

Result

Patient Characteristics

In this study, we investigated the behavior of 246 patients who underwent surgical resection for small-sized lung adenocarcinomas. **Table 1** outlines the demographics and clinical features of the patient population. The majority of patients were female (56.1%), with a median age of 66 years (interquartile Range [IQR]: 56–73 years). Smoking was prevalent in 56.9% of cases. The median maximum tumor diameter on imaging was 1.4 cm (IQR: 1.2–1.6 cm), and the median diameter of the solid component within these tumors was 1.0 cm (IQR: 0.5–1.3 cm). The median consolidation tumor ratio (CTR) was 0.68 (IQR: 0.37–1.00). Surgical procedures predominantly consisted of lobectomies (70.7%), with the remainder being sublobar resections (29.2%).

Pathological evaluation revealed a median tumor diameter of 1.5 cm (IQR: 1.2–1.8 cm) and a median invasion diameter of 0.8 cm (IQR: 0.1–1.5 cm). Lymph node involvement was categorized as pN0 in 93.1% of cases, pN1 in 4.1%, and pN2 in 2.8%. Pathological factors such as lymphatic invasion (ly), vascular invasion (v), pleural invasion (pl), and pleural metastasis (pm) were present in 18.6%, 12.6%, 8.1%, and 2.4% of cases, respectively. The predominant histologic subtypes were AIS and MIA in 7.7% of cases, with invasive adenocarcinoma being the most common (74.4%). The pathological stage distribution was 41.8% at stage 0 and 58.2% at stages IA1-III.

Radiological Factors Analyzed by AI Software in All Patients

The results of the analysis of radiological factors by AI software are shown in **Table 2**. The median whole tumor volume was reported at 1198.7 mm³. The median volumes for GGN and the solid component of tumors were displayed at 596.3 and 362.4 mm³, respectively. The solid component's ratio to the whole tumor was 35.5%. The median maximum diameter of the entire tumor was 15.3 mm. The AI software assigned confidence scores for “solid

Table 2 3D-Radiological parameters analyzed by AI software

Variable	Median	IQR
Whole tumor volume (mm ³)	1198.7	760.7-1710.9
GGN volume (mm ³)	596.3	216.2-1178.3
Solid component volume (mm ³)	362.4	94.8-784.2
Solid component volume ratio (%)	35.5	8.1-76.1
Maximum whole tumor size (mm)	15.3	12.9-17.4
Confidence score of “solid nodule”	0.0069	0.0007-0.9989
Confidence score of “part-solid nodule”	0.0509	0.0002-0.9492
Confidence score of “GGN”	0.0045	2.675e-05-0.5753

nodules” at a median of 0.0069 (IQR: 0.0007–0.9989), “part-solid nodules” at 0.0509 (IQR: 0.0002–0.9492), and “GGN” at 0.0045 (IQR: 2.675e-05–0.5753).

Optimal Threshold Determination for Solid Nodule Classification with K-means Clustering

Figure 2A shows the 3D scatterplot with each dot representing a pulmonary nodule. Each nodule has a confidence score calculated by the AI for the likelihood of solid nodules (AI_solid nodules), part-solid nodules (AI_part-solid nodules), and ground-glass nodules (AI_GGNs). The position of each dot on the plot corresponds to the AI's confidence score for each nodule type, with an axis from 0 (no confidence) to 1 (complete confidence). We utilized the K-means clustering algorithm to process the nodule data, grouping them based on the AI's confidence scores. The clustering effectively sorted the nodules into six distinct categories. This statistical approach allowed us to divide the nodules into distinct groups and determine the exact threshold for classification. Two groups were associated with solid nodules, partially solid GGN, and GGN, respectively. For instance, one group within the solid nodule category exhibited features of a partially solid GGN, and the other group was more distinctly characterized by the attributes typical of solid nodules. The confidence score threshold of 0.87 was determined for the latter group, predominantly characterized by solid nodules. Using cluster

Figure 2 3D scatter plot of AI confidence scores for classifying pulmonary nodules and a representative “Non-AI_solid” pulmonary nodule case. (A) This 3D scatter plot illustrates AI confidence scores for classifying pulmonary nodules as solid (AI_solid), part-solid (AI_part-solid), or ground-glass (AI_GGN). Dots are grouped into 6 categories, each circled by a dashed line, with the “AI_solid” category requiring a confidence score of 0.87 or above. (B) The screenshot demonstrated that AI assigned a confidence score of 0.406 to a solid nodule, which was classified as “Non-AI_solid”.

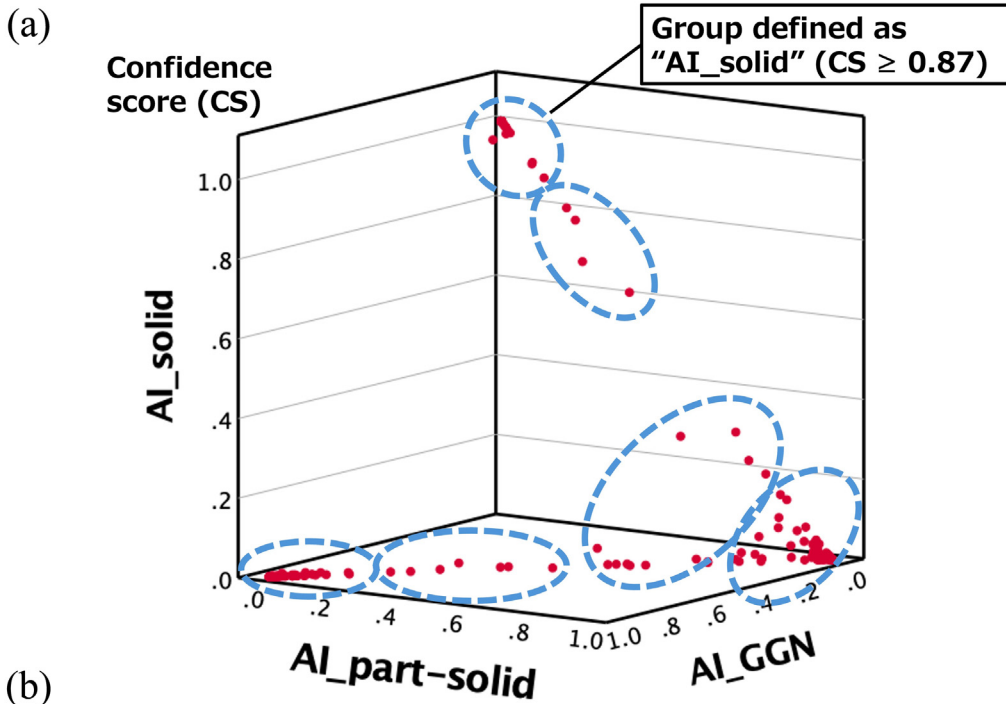
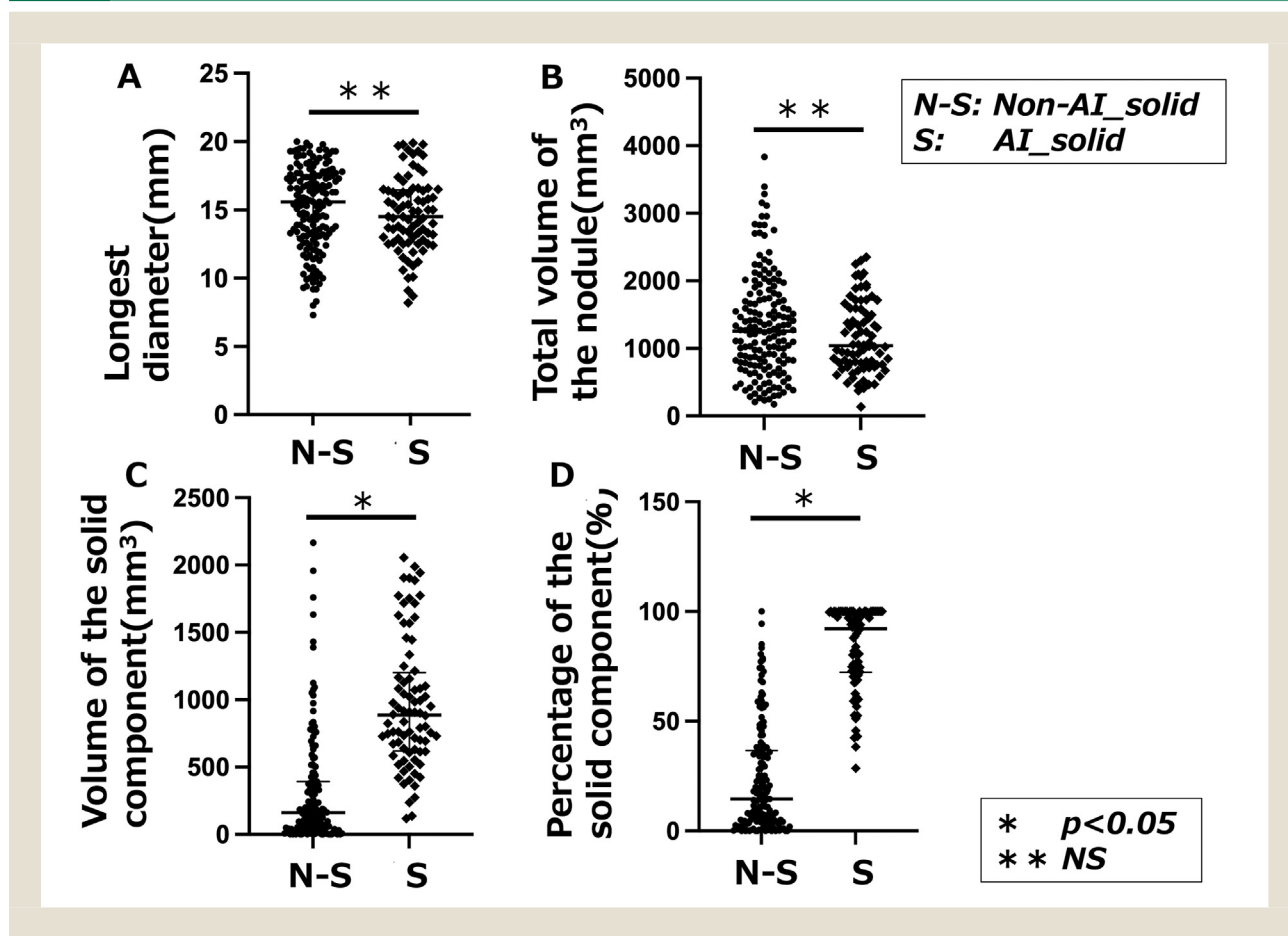


Figure 3 3D-radiological parameters between AI_solid (S) and Non-AI_solid (N-S). (A) compares the median longest diameter. (B) shows the total volume of the nodules. (C) highlights the volume of the solid component. (D) illustrated the percentage of solid component. * $P < .05$; **not significant (NS).



analysis, we focused on groups categorized predominantly as solid nodules. For the following analyses, we defined a confidence score of ≥ 0.87 for a solid nodule determined by the AI as “AI_solid” nodule, and a CS of < 0.87 as a “non-AI_solid” nodule, which the AI determined to be not a solid nodule. Figures 1 and 2B illustrated two representative cases of the confidence score calculated by the AI to classify a nodule as solid, partially solid GGN, or GGN. Figure 1 was classified as AI_solid because the confidence score for a solid nodule was calculated to be 1.000, while Figure 2B had a confidence score of 0.406, which was classified as non-AI_solid.

Comparative Analysis of Nodule Characteristics Based on AI Classification

The characteristics of AI_solid and non-AI_solid nodules are shown in Figure 3. Figure 3A compares the median longest diameter, slightly smaller for AI_solid nodules at 16.3 mm, and non-AI_solid nodules at 14.8 mm, whose difference is not statistically significant (NS). Figure 3B shows the total volume of the nodules; the median volume of AI_solid nodules is 1300 mm³, while that of non-AI_solid nodules is 1100 mm³. Figure 3C highlights the median volume of the solid component, which is 900 mm³ for AI_solid

nodules, significantly higher than the median of 200 mm³ for non-AI_solid nodules ($P < .05$). In Figure 3D, the median percentage of the solid components is higher in AI_solid nodules at 90% compared to only 20% for non-AI_solid nodules ($P < .05$), indicating a significant difference. This result suggests that nodules determined to be AI_solid include those with a volume of a substantial component other than 100%.

Comparative Outcomes of AI_Solid versus Non-AI_Solid Nodules in Predicting Malignancy-Associated Features

Table 3 compares AI-classified AI_solid and non-AI_solid nodules based on the confidence score. The AI_solid group, with a confidence score of ≥ 0.87 , consisted of 80 patients, while the non-AI_solid group included 166 patients with a confidence score < 0.87 . In the AI_solid group, lymph node positivity (pN+) was observed in 16% of patients compared to only 2% in the non-AI_solid group ($P < .001$). A similar trend was noted for lymphatic invasion (ly+), vascular invasion (v+), and pleural invasion (pl+), with significantly higher rates in the AI_solid group (45%, 35%, and 20%, respectively) compared to those of the non-AI_solid group (6%, 2%, and 2%, respectively; all $P < .001$). Upstaging to

Table 3 Comparison of AI_solid versus Non-AI_solid Based on Confidence Score (CS)

Variable	AI_solid (n = 80) (CS ≥0.87)	Non-AI_solid (n = 166) (CS <0.87)	P-value
pN+	13 (16%)	4 (2%)	<.001
ly+	36 (45%)	10 (6%)	<.001
v+	28 (35%)	3 (2%)	<.001
pl+	16 (20%)	4 (2%)	<.001
Upstaging to IA3-IVA	36 (44%)	6 (4%)	<.001
AIS, MIA / Invasive adenocarcinoma	5 (6%) / 75 (94%)	98 (59%) / 68 (41%)	<.001

IA3-IVA was also more common in the AI_solid group at 44% vs. 4% in the non-AI_solid group ($P < .001$). The histologic subtype distribution differed significantly between the two groups, with AIS, and MIA found in 6% of the AI_solid group and 59% of the non-AI_solid group; invasive adenocarcinoma was present in 94% of the AI_solid group compared to 41% of the non-AI_solid group ($P < .001$).

Discussion

This study represents a significant advance in the utilization of AI in CT imaging in the pathological evaluation of small-sized lung adenocarcinoma ≤ 2 cm. Through the application of AI in CT image analysis, tumor size was automatically measured to be ≤ 2 cm and was classified as a solid nodule. Our AI-driven approach made it possible to predict pathologic grades, such as lesions with a high frequency of lymph node metastasis or invasive lung adenocarcinoma, based on these image characteristics. Incorporating AI into the radiological evaluation process enables accurate prediction of lung cancer malignancy and contributes immensely to the treatment strategy.

With increasing attention to the benefits of sublobar resection for small lung cancer, the preoperative evaluation of lymph node metastasis has been highlighted as a crucial factor.^{4,5} In our study, preoperative diagnosis of negative lymph nodes was achieved in all 246 patients using PET/CT imaging. This study design contributed to the validation of the potential of AI analysis of HRCT images to determine “solid nodule” for preoperative assessment of high malignancy in patients who were preoperatively evaluated to have lymph node-negative by PET/CT imaging. Utilization of PET/CT to assess negative lymph nodes and AI analysis of HRCT scans to explore highly malignant lesions can be applied immediately in clinical practice. Furthermore, AI analysis reduced the variability and potential errors characteristic of human interpretation, especially when assessing lesions with GGN, and determined the largest dimension of small lesions. Several physicians have observed that measuring the largest diameter of small pulmonary nodes, especially those ≤ 2 cm, may lead to inter-observer discrepancies, as well as a more significant variation of part-solid nodules. The objectivity provided by AI analysis ensures consistent evaluation.

Several studies on the prognostic differences between lung nodules showed that those containing GGNs are associated with a better prognosis than pure solid nodules.⁹⁻¹⁴ Hattori et al. conducted a central imaging review of 811 cases from a Japanese clinical trial, reporting that approximately 10% of lesions contained GGN, even among those with a CTR of 1.⁹ They compared outcomes between

pure solid lesions and those containing GGN and found significant differences in 5-year overall survival 95.1% vs. 81.1% (log-rank test $P < .0001$) and 5-year recurrence-free survival 93.3% vs. 68.6% ($P < .0001$). They defined radiological semi-consolidation, which exhibits intermediate density between solid and GGO findings, as a part-solid GGN group because it is traditionally considered less invasive and is clinicopathologically similar to lesions with GGN.^{9,26} Furthermore, the frequency of lymph node metastasis in solid nodes was reported to be as high as 17%, similar to our results. It is important to note that PET/CT imaging was not mandatory in the clinical trial data mentioned. This implies that lesions without lymph node enlargement were considered cN0, which might include patients diagnosed with lymph node metastasis if they had undergone PET/CT. Nodules without lymph node enlargement were considered cN0, which may include cases without actual lymph node metastasis. Our study incorporates the diagnosis of lymph node metastasis by PET imaging, which thereby closely reflects current clinical practice.

Our study's strength is in the use of AI to evaluate the characteristics of pulmonary nodules in 3D analysis, especially in the thresholding of the scores derived in determining the nature of the nodules. A critical issue we faced was the appropriate threshold for classifying a nodule as “solid” based on the score generated by the AI. Rather than simply classifying nodules with a score of ≥ 0.5 as “solid,” the K-means clustering method was employed to set a more precise threshold. The nodules that the AI classified as “solid” had nearly 15% lymph node metastasis and high pathologic invasion factors, indicating high-grade malignancy. However, it is crucial to recognize that some of the nodules classified as “substantial” by the AI had minor GGN components in the 3D analysis. This underscores that our approach is not determined by the 3D ratio of GGN to solids but rather depends on the interpretation of the imaging by the AI. Applying AI to analyze pulmonary nodules on CT images, assessing their characteristics, and classifying them as solid nodules based on a specific threshold to indicate potential malignancy, could significantly enhance clinical applications in developing lung cancer treatment strategies.

Although our study highlights the potential of AI in evaluating pulmonary nodules, there were several limitations. Because the study was conducted at a single institution, the broad applicability of our findings is limited, highlighting the need for multicenter study validation. The retrospective design of this study may introduce bias, which may affect the reliability of the results. In addition, the “black box” nature of AI warrants further clarification on features that might be potentially relevant for prediction. In

AI-Driven Solid Nodule for Lung Cancer

In addition, the diagnostic approach to lymph node metastasis incorporates PET/CT scans but only performs EBUS-TBNA for cases in which lymph node metastasis is suspected based on PET results. Despite these limitations, the utilization of AI in our study has the potential to improve the objectivity of decision-making and reduce inter-observer variability, especially in the assessment of nodules with GGN; the statistical calibration of the AI-generated confidence scores enhances the accuracy of this process. In these respects, the clinical application of this system has strong potential to lead to highly accurate diagnoses.

In conclusion, our AI analysis provides a promising approach for automated and objective classification of tumors ≤ 2 cm, including detection of GGN components, and shows potential correlation with malignancy. Drawing on the recent key clinical trials and AI analysis of lung nodules, it would be proposed tailored sublobar resection for small-sized lung cancer based on AI assessment and intraoperative lymph node status. This highlights the need for multicenter prospective trials to validate AI in lung cancer diagnosis and treatment plans and to improve its accuracy in clinical practice.

Clinical Practice Points

- The difficulty in objectively distinguishing solid nodules from nodules containing ground-glass opacities (GGNs), and their differential prognostic impact, poses an important challenge in the preoperative radiological evaluation of pulmonary nodules in lung cancer patients.
- This study highlights the AI-based approach to accurately distinguish these nodule types and indicates its relevance as a preoperative diagnosis of solid nodules for identifying pathologically aggressive lung cancers less than 2 cm in size.
- Drawing from the recent key clinical studies including JCOG0802/WJOG4607L and CALGB140503 and AI insights on pulmonary nodules, we propose tailored sublobar resections for small peripheral lung cancers, guided by AI categorization and intraoperative lymph node status.

Disclosure

The authors declare that they have no known competing financial interests or personal relationships that could have appeared to influence the work reported in this paper.

CRediT authorship contribution statement

Yujin Kudo: Writing – original draft, Visualization, Project administration, Methodology, Investigation, Formal analysis, Data curation, Conceptualization. **Taiyo Nakamura:** Writing – review & editing, Software, Investigation, Formal analysis, Data curation. **Jun Matsubayashi:** Writing – review & editing, Resources, Investigation. **Akimichi Ichinose:** Writing – review & editing, Software. **Yushi Goto:** Writing – review & editing, Resources. **Ryosuke Amemiya:** Writing – review & editing, Resources. **Jinbo Park:** Writing – review & editing, Resources, Investigation. **Yoshihisa Shimada:** Writing – review & editing, Resources. **Masatoshi Kakihana:** Writing – review & editing, Resources. **Toshitaka Nagao:** Writing – review & editing, Resources, Investigation.

Tatsuo Ohira: Writing – review & editing, Supervision, Resources. **Jun Masumoto:** Writing – review & editing, Software. **Norihiko Ikeda:** Writing – review & editing, Supervision, Project administration, Funding acquisition, Conceptualization.

Acknowledgments

We would like to express our gratitude to Mami Murakami for her technical assistance in organizing the data for this study.

Funding

Norihiko Ikeda reports research grant to the Department of Surgery, Tokyo Medical University from FUJIFILM Corporation.

References

1. Sung H, Ferlay J, Siegel RL, et al. Global cancer statistics 2020: GLOBOCAN estimates of incidence and mortality worldwide for 36 cancers in 185 countries. *CA Cancer J Clin.* 2021;71:209–249. doi:10.3322/caac.21660.
2. Moreira AL, Ocampo PSS, Xia Y, et al. A grading system for invasive pulmonary adenocarcinoma: a proposal from the International Association for the Study of Lung Cancer Pathology Committee. *J Thorac Oncol.* 2020;15:1599–1610. doi:10.1016/j.jtho.2020.06.001.
3. Rokutan-Kurata M, Yoshizawa A, Ueno K, et al. Validation study of the international association for the study of lung cancer histologic grading system of invasive lung adenocarcinoma. *J Thorac Oncol.* 2021;16:1753–1758. doi:10.1016/j.jtho.2021.04.008.
4. Saji H, Okada M, Tsuboi M, et al. Segmentectomy versus lobectomy in small-sized peripheral non-small-cell lung cancer (JCOG0802/WJOG4607L): a multicentre, open-label, phase 3, randomised, controlled, non-inferiority trial. *Lancet.* 2022;399:1607–1617. doi:10.1016/S0140-6736(21)02333-3.
5. Altorki N, Wang X, Kozono D, et al. Lobar or Sublobar resection for peripheral stage IA non-small-cell lung cancer. *N Engl J Med.* 2023;388:489–498. doi:10.1056/NEJMoa2212083.
6. Aokage K, Suzuki K, Saji H, et al. Segmentectomy for ground-glass-dominant lung cancer with a tumor diameter of 3 cm or less including ground-glass opacity (JCOG1211): a multicentre, single-arm, confirmatory, phase 3 trial. *Lancet Respir Med.* 2023;11:540–549. doi:10.1016/S2213-2600(23)00041-3.
7. Felip E, Altorki N, Zhou C, et al. Adjuvant atezolizumab after adjuvant chemotherapy in resected stage IB-IIIa non-small-cell lung cancer (IMpower010): a randomised, multicentre, open-label, phase 3 trial. *Lancet.* 2021;398:1344–1357. doi:10.1016/S0140-6736(21)02098-5.
8. Wu YL, Tsuboi M, He J, et al. Osimertinib in resected EGFR-mutated non-small-cell lung cancer. *N Engl J Med.* 2020;383:1711–1723. doi:10.1056/NEJMoa2027071.
9. Hattori A, Suzuki K, Takamochi K, et al. Prognostic impact of a ground-glass opacity component in clinical stage IA non-small cell lung cancer. *J Thorac Cardiovasc Surg.* 2021;161:1469–1480. doi:10.1016/j.jtcvs.2020.01.107.
10. Aokage K, Miyoshi T, Ishii G, et al. Influence of ground glass opacity and the corresponding pathological findings on survival in patients with clinical stage I non-small cell lung cancer. *J Thorac Oncol.* 2018;13:533–542. doi:10.1016/j.jtho.2017.11.129.
11. Nakao M, Oikado K, Sato Y, et al. Prognostic stratification according to size and dominance of radiologic solid component in clinical stage IA lung adenocarcinoma. *JTO Clin Res Rep.* 2022;3:100279. doi:10.1016/j.jtocrr.2022.100279.
12. Watanabe Y, Hattori A, Nojiri S, et al. Clinical impact of a small component of ground-glass opacity in solid-dominant clinical stage IA non-small cell lung cancer. *J Thorac Cardiovasc Surg.* 2022;163:791–801. doi:10.1016/j.jtcvs.2020.12.089.
13. Hattori A, Matsunaga T, Takamochi K, Oh S, Suzuki K. Prognostic impact of a ground glass opacity component in the clinical T classification of non-small cell lung cancer. *J Thorac Cardiovasc Surg.* 2017;154:2102–2110. doi:10.1016/j.jtcvs.2017.08.037.
14. Hattori A, Matsunaga T, Takamochi K, Oh S, Suzuki K. Importance of ground glass opacity component in clinical stage IA radiologic invasive lung cancer. *Ann Thorac Surg.* 2017;104:313–320. doi:10.1016/j.athoracsur.2017.01.076.
15. Saji H, Matsubayashi J, Akata S, et al. Correlation between whole tumor size and solid component size on high-resolution computed tomography in the prediction of the degree of pathologic malignancy and the prognostic outcome in primary lung adenocarcinoma. *Acta Radiol.* 2015;56:1187–1195. doi:10.1177/0284185114554823.
16. Kudo Y, Shimada Y, Matsubayashi J, et al. Artificial intelligence analysis of three-dimensional imaging data derives factors associated with postoperative recurrence in patients with radiologically solid-predominant small-sized lung cancers. *Eur J Cardio-Thorac Surg.* 2022;61:751–760. doi:10.1093/ejcts/ezab541.
17. Shimada Y, Kudo Y, Maehara S, et al. Radiomics with artificial intelligence for the prediction of early recurrence in patients with clinical stage IA lung cancer. *Ann Surg Oncol.* 2022;29:8185–8193. doi:10.1245/s10434-022-12516-x.

18. Kawaguchi Y, Shimada Y, Murakami K, et al. Prognostic impact of artificial intelligence-based volumetric quantification of the solid part of the tumor in clinical stage 0-I adenocarcinoma. *Lung Cancer*. 2022;170:85–90. doi:10.1016/j.lungcan.2022.06.007.
19. Rami-Porta R, Bolejack V, Crowley J, et al. The IASLC lung cancer staging project: proposals for the revisions of the T descriptors in the forthcoming eighth edition of the TNM classification for lung cancer. *J Thorac Oncol*. 2015;10:990–1003. doi:10.1097/JTO.0000000000000559.
20. Brierley J, Gospodarowicz M, Wittekind C, eds. *TNM Classification of Malignant Tumours*. 8th ed. New Jersey, USA: Wiley-Blackwell; 2016:106–112.
21. Momoki Y, Ichinose A, Shigeto Y, Honda U, Nakamura K, Matsumoto Y. Characterization of pulmonary nodules in computed tomography images based on pseudo-labeling using radiology reports. *IEEE Trans Circuits Syst Video Technol*. 2022;32:2582–2591. doi:10.1109/tcsvt.2021.3073021.
22. Momoki Y, Ichinose A, Nakamura K, et al. Development of automatic generation system for lung nodule finding descriptions. *PLoS One*. 2024;19(3):e0300325. doi:10.1371/journal.pone.0300325.
23. Kudo Y, Matsubayashi J, Saji H, et al. Association between high-resolution computed tomography findings and the IASLC/ATS/ERS classification of small lung adenocarcinomas in Japanese patients. *Lung Cancer*. 2015;90:47–54. doi:10.1016/j.lungcan.2015.07.007.
24. Organization WH. *Thoracic tumors*. Lyon, France Geneva, Switzerland: International Agency for Research on Cancer Print copies are distributed by WHO Press, World Health Organization; 2021.
25. Kudo Y, Saji H, Shimada Y, et al. Proposal on incorporating blood vessel invasion into the T classification parts as a practical staging system for stage I non-small cell lung cancer. *Lung Cancer*. 2013;81:187–193. doi:10.1016/j.lungcan.2013.04.016.
26. Suzuki K, Kusumoto M, Watanabe S, Tsuchiya R, Asamura H. Radiologic classification of small adenocarcinoma of the lung: radiologic-pathologic correlation and its prognostic impact. *Ann Thorac Surg*. 2006;81:413–419. doi:10.1016/j.athoracsur.2005.07.058.